


Structural insights into repression of the *Pneumococcal* fatty acid synthesis pathway by repressor FabT and co-repressor acyl-ACP

Gang Zuo, Zhi-Peng Chen, Yong-Liang Jiang, Zhongliang Zhu, Chengtao Ding, Zhiyong Zhang, Yuxing Chen, Cong-Zhao Zhou and Qiong Li 

Hefei National Laboratory for Physical Sciences at the Microscale and School of Life Sciences, University of Science and Technology of China, Hefei, Anhui, China

Correspondence

Q. Li, Hefei National Laboratory for Physical Sciences at the Microscale and School of Life Sciences, University of Science and Technology of China, Hefei, Anhui 230027, China

Tel: +86 551 63600406

E-mail: liqiong@ustc.edu.cn

and

C. -Z. Zhou, Hefei National Laboratory for Physical Sciences at the Microscale and School of Life Sciences, University of Science and Technology of China, Hefei, Anhui 230027, China

Tel: +86 551 63600406

E-mail: zcz@ustc.edu.cn

(Received 18 May 2019, revised 23 June 2019, accepted 1 July 2019)

doi:10.1002/1873-3468.13534

Edited by Stuart Ferguson

The *Streptococcus pneumoniae* fatty acid synthesis (FAS) pathway is globally controlled at the transcriptional level by the repressor FabT and its co-repressor acyl carrier protein (acyl-ACP), the intermediate of phospholipid synthesis. Here, we report the crystal structure of FabT complexed with a 23-bp dsDNA, which indicates that FabT is a weak repressor with low DNA-binding affinity in the absence of acyl-ACP. Modification of ACP with a long-chain fatty acid is necessary for the formation of a stable complex with FabT, mimicked *in vitro* by cross-linking, which significantly elevates the DNA-binding affinity of FabT. Altogether, we propose a putative working model of gene repression under the double control of FabT and acyl-ACP, elucidating a distinct repression network for *Pneumococcus* to precisely coordinate FAS.

Keywords: co-repressor; fatty acid synthesis; repression; transcription repressor

The cell membrane is essential for all living organisms to maintain a stable intracellular environment. Its major components, membrane phospholipids, determine the biophysical property of membrane, which in turn modulates many important membrane-associated functions. Survival of bacteria heavily depends on the homeostasis of membrane phospholipids, especially the ability of tuning phospholipid composition in a rapidly changing environment [1]. Fatty acid synthesis (FAS) plays a key role in the formation of phospholipids [2]. In fact, fatty acid is not only the precursor of

phospholipid synthesis, but also a signal molecule in bacteria [3], making FAS function as a vital facet of bacterial physiology.

Plants and most bacteria adopt the Type II FAS pathway (FAS II) for the *de novo* synthesis of fatty acids [4], which is distinct from its counterpart Type I FAS pathway in insects and mammals [5]. FAS II synthesizes fatty acids *via* a repeated cycle of reactions using a series of mono-functional proteins, each of which is encoded by a discrete gene and catalyzes a single step [6]. In this pathway, all intermediates are

Abbreviations

ACP, acyl carrier protein; FAS II, Type II fatty acid synthesis pathway; FAS, fatty acid synthesis; SFAs, saturated fatty acids; UFAs, unsaturated fatty acids.

shuttled from one enzyme to another by a small acidic protein, termed acyl carrier protein (ACP) [7], which is also responsible for transferring fatty acids to membrane phospholipids [8]. Although FAS II is a fundamental pathway for bacteria, it is a very expensive process from the viewpoint of energy cost. Thus the synthesis of fatty acids should be precisely controlled, especially the ratio of saturated (SFAs) to unsaturated (UFAs) fatty acids [9], to optimize the supply of various membrane phospholipids that match the cell growth. Bacteria have evolved two mechanisms: product feedback inhibition [10] and transcriptional regulation [11]. For example, long-chain acyl-ACP inhibits the activities of acetyl-CoA carboxylase, β -ketoacyl-ACP synthase III, and enoyl-ACP reductase, leading to the termination of chain elongation reactions [12–14]. In contrast, excessive hydrolysis of acyl-ACP upon the high-level expression of thioesterase in *Escherichia coli* leads to the overproduction of fatty acids [15]. However, global regulation at the transcriptional level is a more efficient strategy. Gram-negative bacteria, such as *E. coli*, uses two transcription factors FadR and FabR to regulate the expression of *fabA* and *fabB*, which encode key enzymes required for the synthesis of UFAs [16]. FadR functions as an activator binding to the upstream of *fabA* and *fabB* genes [17,18], whereas FabR is a repressor occupying the promoter regions of these two genes [19]. Nevertheless, Gram-positive bacteria usually utilize a single transcriptional repressor to globally regulate FAS II pathway. For instance, *Bacillus subtilis* FapR binds directly to the promoter region of the FAS regulon and negatively regulates the expression of itself and most genes involved in fatty acid and phospholipid synthesis [20].

The Gram-positive human pathogen *Streptococcus pneumoniae* also possesses a FAS II pathway. The 13 genes involved in the pathway are aligned in a single gene cluster, in which *fabM* encodes an enoyl-ACP isomerase responsible for the synthesis of UFAs [21], whereas *fabK* encodes an enoyl-ACP reductase responsible for the synthesis of SFAs [22]. The synthesis pathway is globally regulated at the transcriptional level by a MarR family repressor, termed FabT [23], which is also conserved in *Enterococcus*, *Clostridium*, and *Lactococcus* [24]. Notably, the *fabT* gene is the second gene in the cluster, just after *fabM*. Biochemical assays showed that FabT regulates *S. pneumoniae* FAS by binding to the DNA palindrome sequence located at the promoter regions of *fabT* and *fabK*, respectively [23]. Inactivation of FabT results in the upregulation of all genes in FAS II pathway except for *fabM* [25]; moreover, the *fabT* knockout strain has a decreased synthesis level of UFAs coupled with an

increase of SFAs [26], suggesting that FabT plays a key role in balancing the ratio of SFAs to UFAs. Rock and colleagues reported that acyl-ACP is the ligand of FabT through a screen of pathway intermediates, but only long-chain acyl-ACP increases the affinity of FabT toward DNA and further represses the expression of downstream genes [27]. Long-chain acyl-ACP is not only a post-translationally modified protein, but also the intermediate of FAS II synthesis and phospholipid synthesis. However, the precise molecular mechanism that regulates FabT activity remains unknown, especially how FabT becomes a stronger brake upon binding to a post-translationally modified protein ligand.

Here, we reported the 2.2 Å crystal structure of FabT in complex with a 23-bp DNA derived from the promoter region of *fabK*. Structural analyses suggested that the apo-form FabT homodimer might adopt a conformation with a low affinity toward DNA. Computational simulations combined with biochemical assays indicated that the long-chain acyl-ACP interacts with FabT *via* inserting the acyl moiety into a tunnel extending from the dimerization domain to the DNA-binding domain, in addition to interactions of the ACP moiety with a basic patch of FabT. The high DNA-binding affinity of a disulfide-linked FabT and ACP complex suggested that acylation of ACP strengthens the interactions with FabT, thus enhances the DNA-binding affinity. Altogether, we proposed a working model of repression of the FAS pathway through a stable complex of FabT and long-chain acyl-ACP.

Materials and methods

Cloning, expression, and purification of FabT and mutants

The coding region of FabT (SPD_0379) was amplified from the genomic DNA of *S. pneumoniae* D39 strain, and cloned into a modified pET28a vector with a 6 × His-tag at the N terminus. The construct was overexpressed in *E. coli* BL21 (DE3) strain (Novagen supplied by Merck, Darmstadt, Germany). The transformed cells were grown at 37 °C to an $A_{600\text{ nm}}$ of 0.7 and then induced with 0.2 mM isopropyl β -D-1-thiogalactopyranoside for a further 4 h before harvesting. Cells were collected by centrifugation (8000 g, 4 °C, 5 min), and resuspended in 30 mL lysis buffer (25 mM Tris-HCl, pH 7.5, 1 M NaCl). After 15 min of sonication and 30 min of centrifugation, the supernatant was loaded onto a Ni-NTA column (GE Healthcare, Chicago, IL, USA) equilibrated with the binding buffer (25 mM Tris-HCl, pH 7.5, 1 M NaCl). The target protein was eluted with 400 mM imidazole and further applied to a Superdex

75 column (GE Healthcare) pre-equilibrated with the binding buffer. The purity of protein was assessed by SDS/PAGE and the protein sample was stored at -80°C .

The selenium-methionine-labeled FabT (SeMet FabT) was overexpressed in *E. coli* B834 (DE3). The transformed cells were grown at 37°C in SeMet medium (M9 medium supplemented with $50\text{ mg}\cdot\text{L}^{-1}$ SeMet and other essential amino acids at $50\text{ mg}\cdot\text{L}^{-1}$) to an $A_{600\text{ nm}}$ of 0.7. The following steps in protein expression and purification were the same as those for the native protein. Site-directed mutagenesis was performed using the MutExpress™ Fast Mutagenesis Kit (Vazyme Biotech, Nanjing, China) with the plasmid encoding the wild-type FabT as the template. The mutant protein was expressed, purified and stored in the same manner as the wild-type protein.

Crystallization, data collection, and processing

The protein was concentrated to $12\text{ mg}\cdot\text{mL}^{-1}$ for crystallization by ultrafiltration (Millipore Amicon, Bedford, MA, USA). The single-stranded DNA was synthesized by Sangon Biotech (Shanghai, China), and resuspended in the buffer containing 25 mM Tris-HCl, pH 7.5, and 50 mM NaCl. Complementary DNA strands were heated at 95°C for 5 min and then annealed slowly to room temperature. The recombinant FabT and duplex DNA were mixed at a molar ratio of 1 : 1.1, and then applied to crystallization.

Crystals of FabT–DNA complex were grown at 289 K using the hanging drop vapor diffusion method, with a drop of $1\ \mu\text{L}$ protein–DNA solution mixed with an equal volume of the reservoir solution (5% polyethylene glycol 4000, 0.2 M sodium acetate, 0.1 M sodium citrate, pH 5.5). After optimization, crystals were transferred to cryoprotectant (reservoir solution supplemented with 30% glycerol) and flash-cooled with liquid nitrogen. The x-ray diffraction data were collected at 100 K in a liquid nitrogen stream using beamline BL17U with an Eiger X 16M detector at the Shanghai Synchrotron Radiation Facility. The diffraction data were indexed, integrated, and scaled with the program HKL2000 [28].

Structure determination and refinement

The crystal structure of FabT complexed with a 23-bp DNA was determined using the single-wavelength anomalous dispersion method [29]. The AutoSol program implemented in PHENIX [30] was used to search the selenium atoms and to calculate the phase. Then, automatic model building was carried out by the program AutoBuild in PHENIX. The initial model was further refined by the maximum likelihood method in REFMAC5 [31] of CCP4i program suite and rebuilt interactively with the program COOT [32]. The final model was evaluated with the web service MolProbity [33]. The crystallographic parameters were listed in Table 1. The $|F_o| - |F_c|$ omit electron density map is

countered at $3.0\ \sigma$ was calculated by PHENIX. All structure figures were prepared with PyMOL (<https://pymol.org>).

Electrophoretic mobility shift assays (EMSA)

The oligonucleotides labeled with 6-carboxyfluorescein (6-FAM) at the 5'-end were synthesized by Sangon Biotech. The DNA probes were incubated with the proteins in the binding buffer (20 mM Tris-HCl, pH 7.5, 50 mM NaCl) for 30 min on the ice. The competitor poly(dI-dC) was added for eliminating the nonspecific DNA binding. The final concentrations of proteins, DNA probes, and ligands were 300, 40, and 600 nM, respectively. The mixture was

Table 1. Data collection and structure refinement statistics

	Se-FabT + 23-bp DNA	FabT + 23-bp DNA
Data collection		
Space group	$P2_1$	$P2_1$
Cell dimensions		
<i>a</i> , <i>b</i> , <i>c</i> (Å)	73.22, 61.49, 73.90	73.02, 60.86, 74.08
α , β , γ ($^{\circ}$)	90.00, 105.75, 90.00	90.00, 105.40, 90.00
Resolution (Å)	50.00–2.45 (2.54–2.45) ^a	50.00–2.20 (2.28–2.20) ^a
Unique reflections	23,174 (2,248)	31,594 (3,169)
Completeness (%)	98.2 (99.8)	98.5 (100)
$ I/\sigma $	14.7 (3.8)	18.1 (3.5)
R_{sym} (%)	14.6 (69.9)	8.5 (54.0)
Redundancy	5.7 (4.8)	6.2 (6.0)
Refinement		
Resolution (Å)		35.93–2.20
NO. reflections		31534
$R_{\text{work}}/R_{\text{free}}$ (%)		18.76/22.07
NO. atoms		
Protein		2370
DNA		935
Water		209
B factors (Å ²)		
Protein		43.14
DNA		49.48
Water		49.93
R.m.s deviations		
Bond lengths (Å)		0.010
Bond angles ($^{\circ}$)		1.445
Ramachandran plot (residues, %)		
Most favored		99.30
Allowed		0.70
Outliers		0
PDB entry		6JBX

^aHighest resolution shell is shown in parenthesis. $R_{\text{sym}} = \sum_i \sum_j |I_{ij} - I_i| / \sum_i \sum_j I_{ij}$, where I_i is the mean intensity of the i observations of symmetry related reflections of h . $R = \sum |F_{\text{obs}} - F_{\text{calc}}| / \sum F_{\text{obs}}$, where $F_{\text{obs}} = F_{\text{p}}$, and F_{calc} is the calculated protein structure factor from the atomic model. Rmsd in bond lengths and angles are the deviations from ideal values.

separated by 8% native-PAGE, and then the gel was visualized through fluorescence imaging using IMAGEQUANT LAS 4000 (GE Healthcare).

Synthesis of the long-chain acyl-ACP

The long-chain acyl-ACP was synthesized *in vitro* using a two-step enzymatic reaction. Usually, the substrate protein ACP purified from the *E. coli* cells is an inactive form, namely apo-ACP. The holo-ACP synthase catalyzes the transfer of 4'-phosphopantetheine group from CoA to Ser38 of apo-ACP, thus converting apo-ACP to holo-ACP [34]; whereas the acyl-ACP synthetase catalyzes the ligation of fatty acid to the 4'-phosphopantetheinyl moiety of holo-ACP to produce long-chain acyl-ACP [35].

The *S. pneumoniae* ACP (SPD_0044) was cloned into a pET22b-derived vector without 6 × His-tag, and overexpressed in *E. coli* BL21-Ril (DE3) strain (Novagen). The supernatant containing the target protein was first loaded onto a HiTrap™ QFF column (GE Healthcare), and then the ACP protein was further purified using a Superdex 75 10/300 GL column (GE Healthcare) equilibrated with the reaction buffer (20 mM Tris-HCl, pH 7.5, 100 mM NaCl). Samples for the enzymatic reaction were collected at the highest peak fractions of gel filtration and stored at −80 °C. The ACP mutants and the holo-ACP synthase from *S. pneumoniae* were expressed and purified in the same manner as wild-type ACP, whereas the *E. coli* acyl-ACP synthetase was expressed and purified in a way similar to FabT. A reaction mixture of 100 μL containing 100 μM CoA, 100 μM apo-ACP, and excess holo-ACP synthase in the reaction buffer was incubated at 37 °C for 30 min; Then a twofold molar mass of cis-vaccenate and excess acyl-ACP synthetase was added and incubated at 37 °C for another 3 h, leading to the synthesis of cis-vaccenoyl-ACP (18 : 1Δ11-ACP). The product of each step was identified by Tricine-PAGE.

Molecular docking

The structure of ACP was gained by homology modeling based on *Enterococcus faecalis* AcpB (PDB code: 2N50). Then, the simulated ACP was docked onto the FabT-DNA-complexed structure using HADDOCK2.2 [36]. HADDOCK generated 165 structures in three clusters, which cover 82.5% of the water-refined models. The best cluster, which represents the most reliable model, possesses a HADDOCK score of −123.8 (±6.2), a Z score of −1.2 and a RMSD value of 1.5 (±0.4) Å.

SDS/PAGE analysis and preparation of FabT-ACP complex

The FabT-ACP complex, linked *via* an intermolecular disulfide bond, was prepared according to previous reports

[37]. FabT^{K97C} and ACP^{D50C} were purified and reduced by 4 mM DTT before desalting, respectively. Then, FabT^{K97C} was incubated with a 10-fold molar excess of 5,5'-dithiobis-(2-nitrobenzoic acid) (DTNB) at 25 °C for 30 min to introduce a disulfide bond between Cys97 of FabT and thionitrobenzoic acid (TNB). After removing the excess DTNB, three samples were prepared (FabT^{K97C}-TNB, ACP^{D50C} and FabT^{K97C}-TNB+ACP^{D50C}) and incubated at 25 °C for 30 min. Each sample was divided into two parts with or without 4 mM DTT, and applied to SDS/PAGE to detect the formation of disulfide bond. For preparation of FabT^{K97C}-ACP^{D50C} complex, FabT^{K97C}-TNB was incubated with fourfold molar excess ACP^{D50C}. Then, the complex was purified by Ni-NTA column (with the 6 × His-tag of FabT^{K97C}) and Superdex 75 100/300 column (GE Healthcare) to remove the non-crosslinked FabT^{K97C} and the excess ACP^{D50C}.

Results

Crystal structure of the FabT-DNA complex

Previous report had proved that FabT showed a higher affinity toward a perfect palindromic sequence 5'-AGTTTGACTGTCAAATT located in the *fabK* promoter compared to the sequence 5'-GTTTTGATTGTAAAAGT in the *fabT* promoter [27]. Thus we co-crystallized FabT with DNA duplexes of varying lengths derived from the *fabK* promoter. After crystal screening and optimization, we found a diffraction quality crystal from the complex with a 23-bp duplex DNA fragment, and solved the structure at 2.2 Å resolution in the space group *P2₁* (Table 1).

In the structure, each asymmetric unit contains an intertwined, pyramidal FabT homodimer binding to a 23-bp duplex DNA (Fig. 1). Despite sharing a low identity of primary sequence, FabT adopts a tertiary structure similar to other MarR family members of known structure [38]. Each subunit comprises six α helices and two β strands, which are arranged with a topology in the order α1-α2-α3-α4-β1-β2-α5-α6, and folded into two functional domains: a dimerization domain and a winged helix-turn-helix (wHTH) domain (Fig. 1). The dimerization domain, which is formed by the N-terminal helix α1 and the C-terminal helices α5 and α6 from both subunits, locates at the apex of the pyramidal structure (Fig. 1). Helix α1 of one subunit and helices α5' and α6' of the other subunit intertwine with each other, making FabT a highly compact and stable dimer, which buries a total interface area of ~ 5000 Å² as calculated by PDBe-PISA (www.ebi.ac.uk/pdbe/pisa/). The internal faces of the dimerization domain are hydrophobic, a feature conserved in MarR

homologs [39], and mutations of the related residues would attenuate the DNA-binding affinity [40]. The wHTH domain, responsible for DNA binding, is composed of helices $\alpha 2$, $\alpha 3$, and $\alpha 4$, and an additional winged motif, which consists of an antiparallel β -hairpin $\beta 1$ - $\beta 2$ (Fig. 1). The two wHTH domains are located at the base of the pyramidal architecture, and clip the double-stranded DNA on both sides like a hook. Each FabT subunit interacts with half of the 23-bp DNA *via* inserting the recognition helix $\alpha 4$ into DNA major groove, and the loop of the winged motif into the flanking minor groove (Fig. 1). The two recognition helices are apart from each other of approximately 26 Å, binding to a successive DNA major groove. The winged motif is a signature of MarR family transcription factors, which is highly flexible and invisible in most crystal structures in the absence of DNA [41]. Notably, we found two long strips of electron density almost symmetrically located at the dimerization domain of our structure (Fig. 1), each of which possibly fits a fatty acid chain of about 13 carbons in length, reminiscent us of a homolog of the acyl moiety of ligand.

DNA-binding pattern

FabT dimer forms a complex with the 23-bp DNA duplex at a molar ratio of 1 : 1. The parameters calculated by 3DNA server [42] indicated that the DNA in our structure adopts a deformed B-DNA conformation upon binding to FabT, with a slightly enlarged major groove of 12.1 Å in width compared to the ideal B-DNA of 11.7 Å. The two wHTH domains of FabT dimer, especially the winged motif clustering of basic residues, are positively charged and thus complementary

to the duplex DNA. As the 23-bp DNA is a palindromic sequence, the two interfaces between DNA and FabT are symmetric (Fig. 2A).

In detail, the side chains of Thr65, Thr67, and Asn71 on the recognition helix $\alpha 4$ form hydrogen bonds with the sugar-phosphate backbone of c15', t6, and t7, respectively; whereas the side chain of Arg81 and main chains of Arg88 and Val91 on the winged motif form hydrogen bonds with the sugar-phosphate backbone of t6, t23', (or g23 on the other interface) and g5, respectively (Fig. 2B). Moreover, the side chain of Arg89 at the tip of the winged motif forms hydrogen bonds with the base groups of t3 and t22' (Fig. 2B). Indeed, mutation of the conserved residue Arg89 resulted in a decreased DNA-binding affinity [43]. In addition, four residues Ser34, Lys36, Ser53, and Thr62 on the wHTH domain interact with the phosphate groups of DNA to further stabilize the FabT-DNA complex (Fig. 2B).

A search against the DALI database [44] revealed that FabT has a highest structural homology to MexR-R21W mutant (PDB code: 4ZZL, Z score 15.7, RMSD 3.2 Å over 239 C α atoms, sequence identity 18%). MexR is a repressor of the MexAB-OprM efflux pump in *Pseudomonas aeruginosa* [45], the R21W mutant of which can stabilize the protein at a non-DNA-binding ground state [46]. It suggested that FabT in our structure adopts a looser binding mode, despite forming a complex with DNA. Comparison with those DNA-complexed structures in the output of DALI search indicated that the 24-bp DNA-complexed MepR, a repressor of *Staphylococcus aureus* multidrug efflux operon *mepRA* [47], has the highest Z score (PDB code: 4LLN, Z score 15.4, RMSD 2.9 Å over 266 C α atoms, sequence identity 23%).

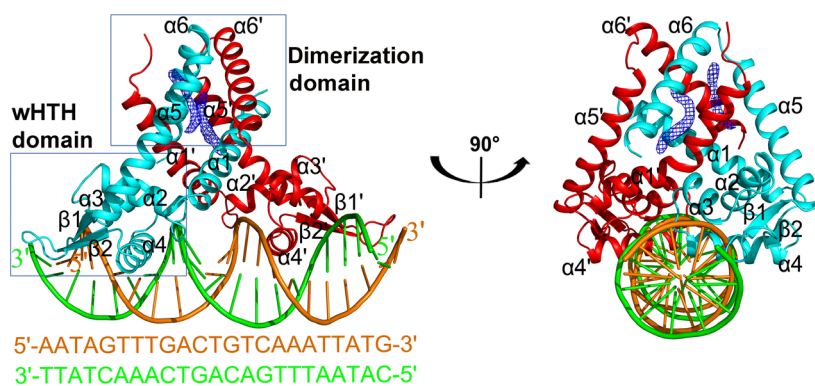


Fig. 1. Overall structure of FabT dimer in complex with the 23-bp duplex DNA derived from the *fabK* promoter. The two subunits are colored in cyan and red, respectively. The secondary structural elements of each subunit are labeled sequentially. The dimerization domain and wHTH domain are highlighted in black rectangle, respectively. The long strip of electron density is counteracted at 3.0 Å level. The duplex DNA strands are colored in orange and green, respectively. wHTH stands for winged helix-turn-helix.

Superposition revealed that the recognition helix $\alpha 4$ of FabT inserts into the DNA major groove not as deep as that in MepR-DNA structure (Fig. 3), further indicating that FabT might have a weaker interaction with DNA. Analyses by PDBe-PISA showed that FabT has a buried interface area of 3600 \AA^2 with DNA smaller than that of MepR at 3890 \AA^2 . Further superposition indicated most other DNA-complexed structures of MarR family members deposited in PDB (<https://www.rcsb.org/>) have a recognition helix $\alpha 4$ inserting into the DNA major groove much deeper, compared to that in the FabT-DNA complex. All together, FabT probably adopts a conformation at a low affinity toward DNA in the absence of ligand.

Enhanced DNA-binding affinity upon binding to acyl-ACP and a putative model of the FabT-ACP complex

The fatty acid 18 : 1 Δ 11-ACP, which is most abundant in *S. pneumoniae* membrane phospholipids [27], was catalytically synthesized *in vitro* using a two-step enzymatic reaction, and verified by Tricine-PAGE. The shift due to the adduct of 4'-phosphopantetheinyl group and acyl chain indicated the production of holo-ACP and acyl-ACP, respectively (Fig. 4A). But since the molecular weights of 4'-phosphopantetheinyl group and acyl chain are small, the band shifts are not very obvious. The DNA-binding abilities of FabT in the presence of various products were analyzed by

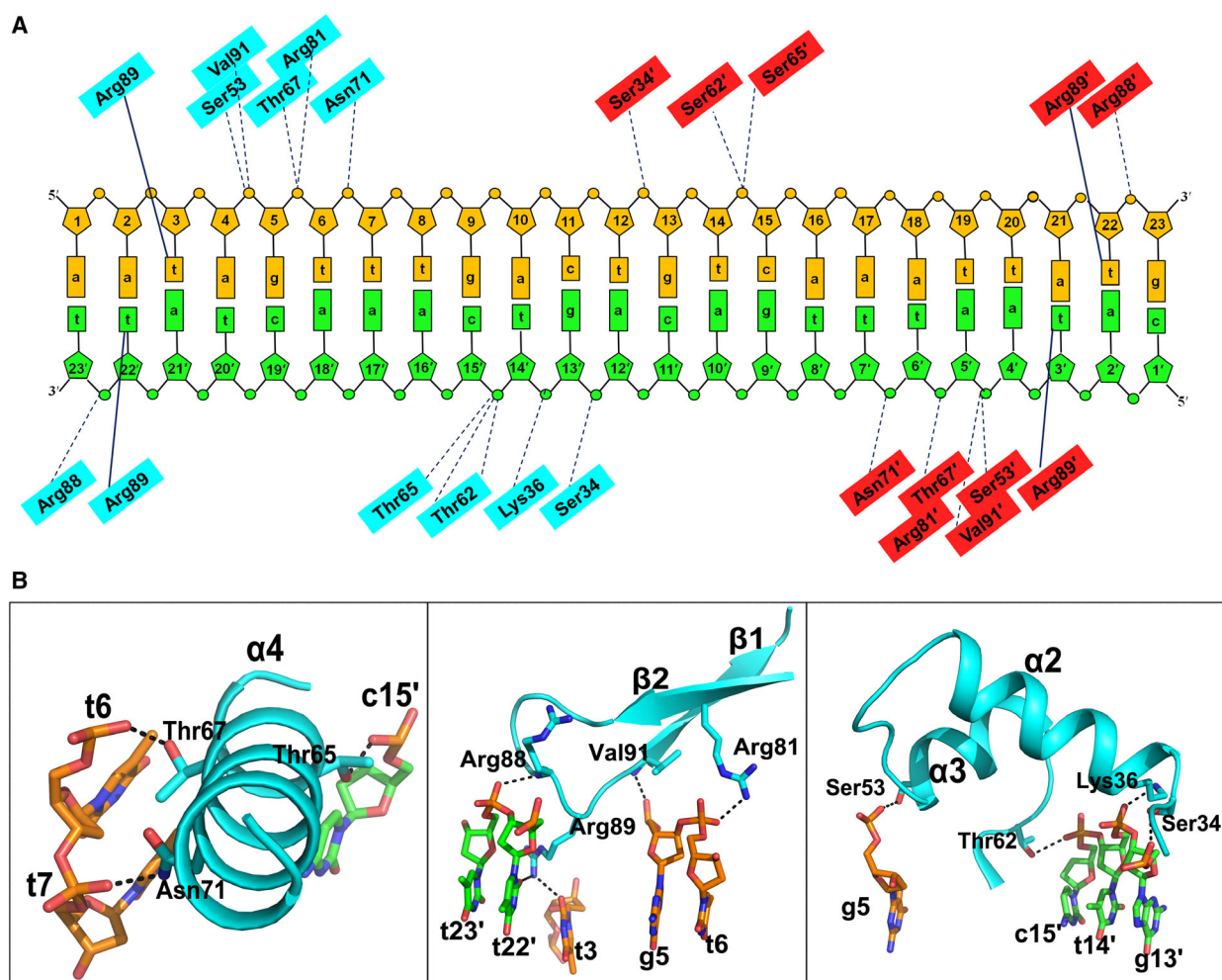
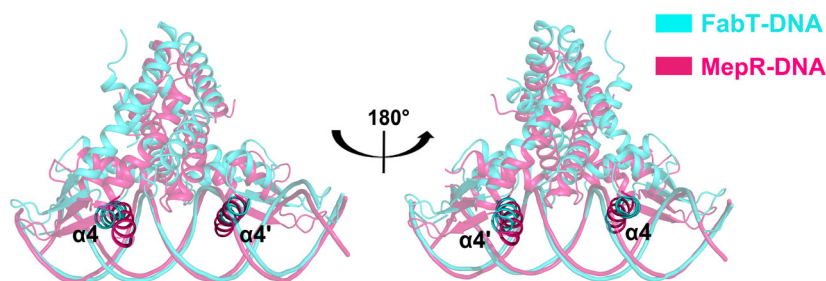


Fig. 2. DNA-binding pattern of FabT. (A) Schematic representation of interaction networks between FabT and DNA. Interacting residues are marked with the same color as their corresponding subunits, respectively. The DNA strands are displayed as orange and green, respectively. Solid lines indicate hydrogen bonds between FabT and base groups of DNA, whereas dashed lines indicate interactions between FabT and sugar-phosphate backbone of DNA. (B) Cartoon representation of the contacts between FabT and corresponding nucleotides. The involved residues and nucleotides are labeled and shown as sticks. The dashed lines represent hydrogen bonds.

Fig. 3. Structural superposition of *Streptococcus pneumoniae* FabT-DNA (cyan) on *Staphylococcus aureus* MepR-DNA (hotpink; PDB code: 4LLN). The recognition helices $\alpha 4$ and $\alpha 4'$ of FabT dimer are highlighted and labelled.



EMSA. A final concentration of FabT up to 300 nM could not trigger the band shift of DNA, even in the presence of apo-ACP or holo-ACP (Fig. 4B, lanes 1–4). Upon the addition of acyl-ACP, significant band shift could be seen from the gel; and moreover, the DNA-binding band becomes stronger along the increase of acyl-ACP concentration (Fig. 4B, lanes 5–8). The results are coincident with the previous report [27], indicating that long-chain acyl-ACP could enhance the DNA-binding affinity of FabT, which corresponds to the low affinity of FabT toward DNA in the absence of acyl-ACP. It is the only example in MarR family with a co-repressor of post-translationally modified protein ligand. Besides, the assays provide a platform for further investigation of interaction mode between FabT and acyl-ACP. Notably, *S. pneumoniae* encodes two isoforms of ACP: namely SPD_0381 and SPD_0044, which are in the FAS II gene cluster and an operon encoding phosphate acyl-transferase PlsX, which is involved in phospholipid synthesis. We purified both isoforms and found that only acyl-SPD_0044, but not acyl-SPD_0381, increases the DNA-binding affinity of FabT. Thus only ACP/SPD_0044 was applied to all experiments.

To gain the structural insights into the enhanced DNA-binding affinity with the help of co-repressor, we tried to solve the tertiary structure of FabT, acyl-ACP and DNA, but did not succeed. Alternatively, we performed docking experiments to build a complex model. The electrostatic potential analysis revealed that each FabT subunit possesses a highly basic patch (Fig. 4C), besides a basic region responsible for binding DNA. Interestingly, *S. pneumoniae* ACP has a rather negatively charged surface (Fig. 4C), as shown in a modeled structure based on the 50% sequence-identical *E. faecalis* AcpB (PDB code: 2N50). It strongly suggested that FabT and apo-ACP might form a complex *via* interactions between the complementary basic patch and acidic surface. Simulation with HADDOCK2.2 [36] enabled us to build a stable complex of FabT-ACP with a buried interface area of $\sim 1110 \text{ \AA}^2$ on each side (Fig. 4D). In the modeled complex, two ACP molecules symmetrically bind to FabT dimer on

the two basic patches (Fig. 4D). A close look revealed that the positively charged residues on helix $\alpha 5$ of FabT form salt bridges with the negatively charged residues along the helix $\alpha 2$ of ACP.

Multiple-sequence alignment suggested that the positively charged residues on helix $\alpha 5$ are highly conserved in FabT and homologs. However, single mutation of the conserved residues Lys97, Arg100, or Arg104 slightly altered the DNA-binding affinity of FabT in the presence of 18 : 1 $\Delta 11$ -ACP (Fig. 4E). In contrast, the double mutation with K97A&R100A almost resulted in the loss of DNA-binding ability (Fig. 4E). It indicated that FabT could tightly bind ACP, and further proved the reliability of FabT-ACP complex model.

Applying the structure to the program CAVER [48] revealed a tunnel that starts at the cleft composed of helices $\alpha 1$, $\alpha 5'$, and $\alpha 6'$, runs along helix $\alpha 1$ and helix $\alpha 5'$, and finally reaches the wHTH domain (Fig. 4F). This tunnel is hydrophobic, and provides a similar space that is occupied by the putative fatty acid chain in our structure (Fig. 1). Moreover, the 4'-phosphopantetheinyl moiety could be well accommodated between the tunnel entrance and the active site Ser38 of ACP. It indicated that the hydrophobic tunnel is most likely the binding pocket of the acyl moiety of ligand.

A stable complex of FabT-ACP is necessary for the enhanced DNA-binding affinity

As shown in Fig 4B, only acyl-ACP, neither holo-ACP nor apo-ACP, can significantly enhance the DNA-binding affinity of FabT, despite FabT interacts with apo-ACP *via* a line of salt bridges (Fig. 4D). It indicated that the post-translational modification of ACP with an acyl chain contributes more hydrophobic interactions with the hydrophobic tunnel of FabT, and form a relatively stable complex of FabT-(acyl-ACP) that gains higher DNA-binding affinity. To validate this hypothesis, we mutated several pairs of residues at the interface between FabT and ACP to cysteines for introducing the intermolecular disulfide bond. As

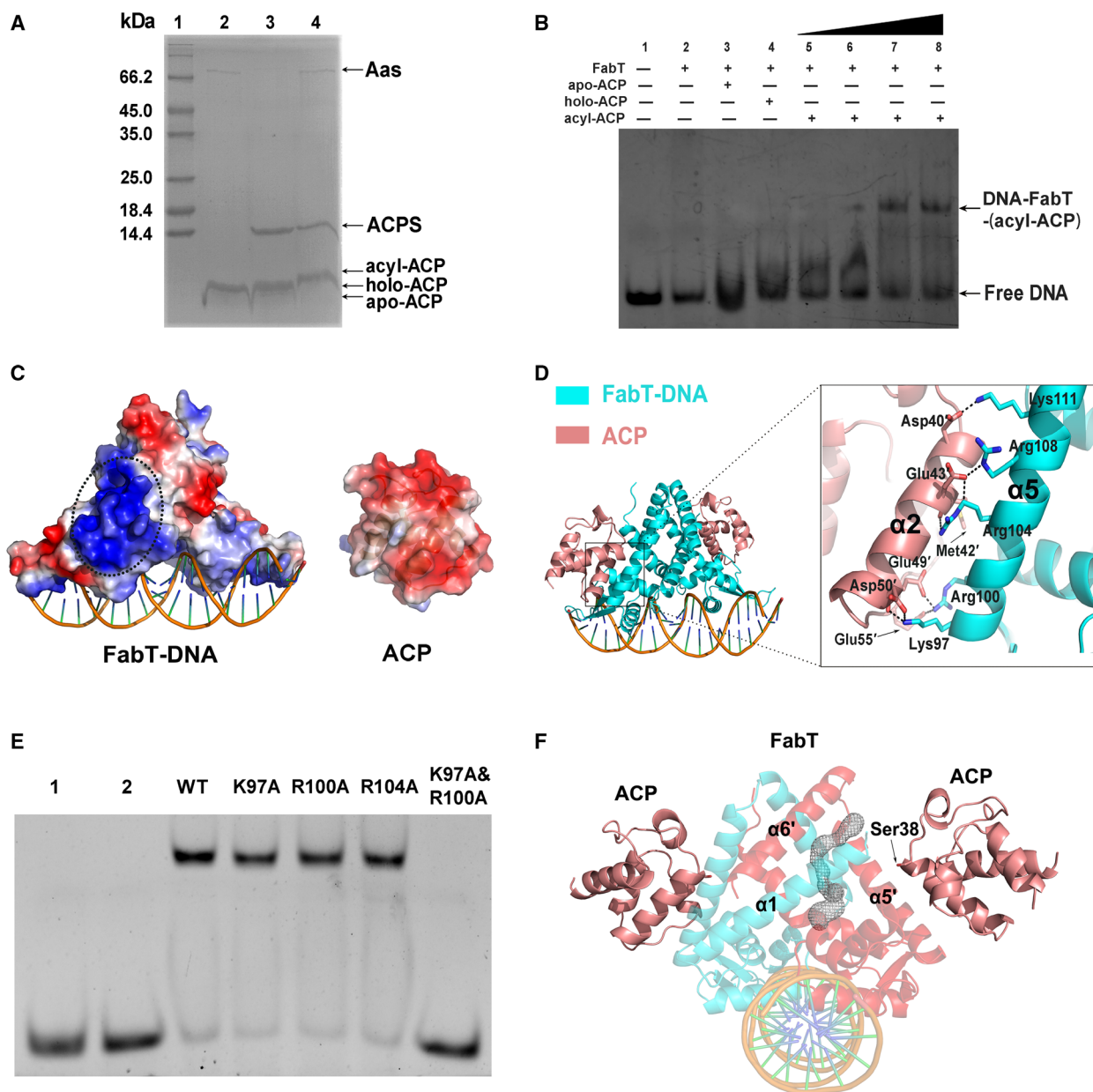


Fig. 4. The complex of FabT and ACP. (A) Tricine-PAGE analysis of the reaction products of acyl-ACP synthesis. Lane 1: protein marker; lane 2: apo-ACP; lane 3: the production of holo-ACP; lane 4: the production of acyl-ACP. ACPS: holo-ACP synthase; Aas: acyl-ACP synthetase. (B) EMSA assays of FabT with DNA in the presence of different ligands. The concentrations of FabT and DNA are 300 and 40 nM, respectively. FabT with and without ligands are shown as '+' and '-', respectively. The concentration of apo-ACP or holo-ACP is 600 nM. The concentrations of 18:1 Δ 11-ACP in lane 5 to lane 8 are 50, 150, 300, and 600 nM, respectively. (C) Electrostatic potential diagrams of FabT and ACP. The structure of *Streptococcus pneumoniae* ACP is gained by homology modeling based on *Enterococcus faecalis* AcpB (PDB code: 2N50). The positively charged patch of FabT is indicated by dashed oval. (D) A docking model of FabT-DNA binding to ACP. The inset shows a close-up view of the interface. The interacting residues are labeled and shown as sticks. Dashed lines indicate salt bridges. (E) EMSA assays of FabT (WT) and mutants (K97A, R100A, R104A, and K97A & R100A) with DNA in the presence of 18:1 Δ 11-ACP. Lane 1: free DNA; lane 2: negative control, DNA incubated with FabT in the absence of 18:1 Δ 11-ACP. (F) The putative ligand-binding tunnel in the FabT-DNA structure. The tunnel was calculated by the program CAVER 3.0.1 and shown in mesh.

expected, mutation of two pairs of residues worked the best: FabT^{K97C}-ACP^{D50C} and FabT^{R108C}-ACP^{E43C}, the former of which was applied to further assays. A

disulfide-linked complex of FabT^{K97C}-ACP^{D50C} could be observed in the absence of reductant DTT (Fig. 5A, lane 7); and moreover, the complex could be

dissociated upon addition of DTT (Fig. 5A, lane 3). Notably, most of the input FabT^{K97C} and ACP^{D50C} form a stable disulfide-linked complex, which is proved by LC-MS. It further indicated that FabT is able to bind to ACP in solution.

Then, the complex of FabT^{K97C}-ACP^{D50C} linked by an intermolecular disulfide bond was purified using Ni-NTA affinity chromatography followed by gel filtration, and applied to EMSA assays. Compared to apo-form FabT at the same molarity, which could not form a retarded band with DNA (Fig. 5B, lane 2), the complex FabT^{K97C}-ACP^{D50C} binding to DNA form an apparent retarded band (Fig. 5B, lane 4), which is comparable to the complex of FabT and long-chain acyl-ACP binding to DNA (Fig. 5B, lane 3). In addition, along with the increase in input FabT-ACP complex, more and more FAM-labeled DNA was shifted upon formation a ternary complex with FabT-ACP (Fig. 5B, lanes 4–6). Moreover, in the presence of DTT, which reduces the disulfide bond between FabT^{K97C} and ACP^{D50C}, only FabT at a concentration up to 400 nM can form retarded band with DNA (Fig. 5B, lanes 7–9). Notably, given a different size, the ternary complex FabT-ACP-DNA could be easily distinguished from the binary complex FabT-DNA. Altogether, it suggested that modification of ACP with a long-chain fatty acid helps ACP to form a stable complex with FabT, which could be mimicked by introducing an intermolecular disulfide bond, and elevates the DNA-binding affinity of FabT.

Discussion

Precise regulation of FAS is essential for maintaining the homeostasis of cell membrane, thus crucial for

the growth and survival of bacteria. *S. pneumoniae* employs FabT, a MarR family transcription factor, to globally regulate the FAS pathway [23]. MarR family members, which are characterized with a conserved wHTH domain, are widespread in all prokaryotes from archaea to bacteria. The family was originally named after *E. coli* MarR, a repressor of the *marRAB* operon, the products of which confer resistance to multiple antibiotics and household disinfectants [49]. Usually, the DNA-binding affinity of MarR family members are subject to regulation *via* diverse small ligands, such as phenolic molecules and metals, or of post-translational modifications, resulting in upregulation of related genes in most cases [43]. This fine regulatory mechanism enables bacteria to respond to various environmental stimuli timely and properly [50].

Unlike other MarR family members, FabT utilizes a post-translationally modified protein ligand, the long-chain acyl-ACP as a co-repressor. However, the regulatory mechanism remains unclear. Indeed, the *S. pneumoniae* D39 genome contains two annotated *acp* genes, namely *spd_0381* and *spd_0044*, sharing a primary protein sequence identity of 40%. We found that SPD_0044, not SPD_0381, after being modified with the long-chain acyl moiety, could enhance the DNA-binding affinity of FabT. Notably, a recent report found that acyl-AcpB in *E. faecalis*, which is counterpart of *S. pneumoniae* SPD_0044, is a more potent regulatory ligand of FabT [51]. Moreover, gene knockout assays showed that *E. faecalis* FabT functions in a manner similar to that of *S. pneumoniae* FabT [51]. Thus we speculated that acyl-SPD_0044 is more likely the physiological ligand of FabT in *S. pneumoniae*.

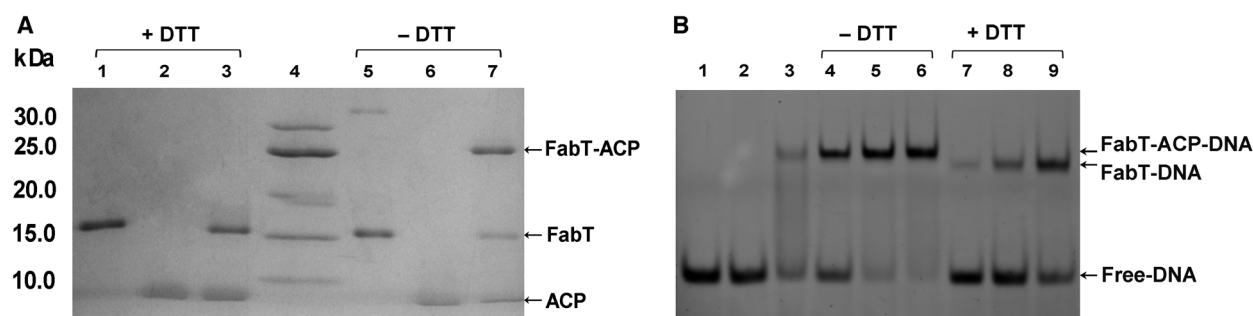


Fig. 5. A stable FabT-ACP complex enhances FabT binding to DNA. (A) electrophoresis of the complex between FabT^{K97C} and ACP^{D50C}. The Coomassie-stained gel shows the formation of intermolecular disulfide bond between FabT^{K97C} and ACP^{D50C} after incubation under nonreducing conditions. Lanes 1–3: FabT^{K97C}, ACP^{D50C}, and FabT^{K97C}+ACP^{D50C} with 4 mM DTT; lane 4: protein marker; lanes 5–7: samples corresponding to lanes 1–3, respectively, without DTT. (B) EMSA assays of FabT^{K97C}-ACP^{D50C} complex with or without DTT. Lane 1: free DNA; lane 2: negative control, DNA incubated with FabT in the absence of acyl-ACP; lane 3: positive control, DNA incubated with FabT in the presence of acyl-ACP; lanes 4–6: DNA incubated with various concentrations (300, 350 and 400 nM) of FabT-ACP complex in the absence of DTT; lanes 7–9: samples corresponding to lanes 4–6, respectively, in the presence of 4 mM DTT.

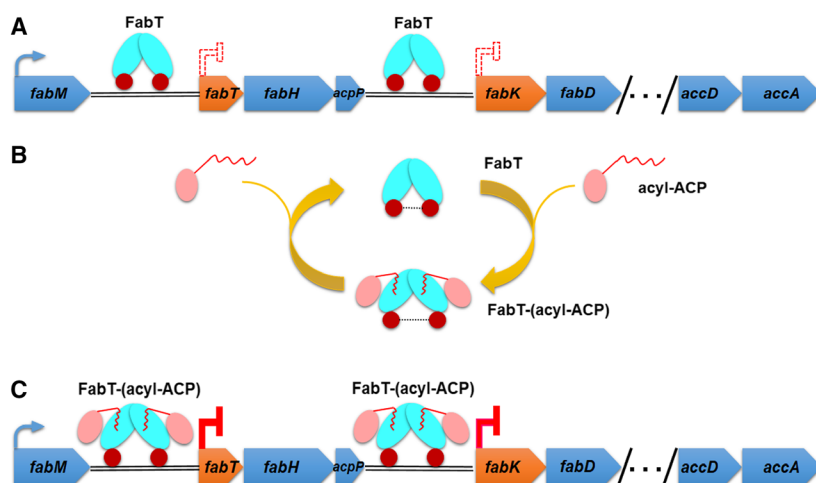


Fig. 6. A model of repressor FabT working together with co-repressor acyl-ACP. (A) FabT binds to the promoter regions of *fabT* and *fabK* as a weak repressor. (B) FabT forms a stable complex with the long-chain acyl-ACP and undergoes conformational changes. (C) The stable FabT-(acyl-ACP) complex tightly binds to the promoter regions of *fabT* and *fabK* as a strong brake.

Based on our structural analyses and biochemical assays, in combination with the recent report [51], we propose a working model of gene repression by FabT together with the ligand. Under normal circumstance, FabT is constitutively expressed and loosely binds to the promoter regions of *fabT* and *fabK*, and partly represses the expression of 12 genes in the FAS operon except for *fabM*. In consequence, the leaky expression of the FAS operon maintains the *de novo* FAS at a basal level (Fig. 6A). When *S. pneumoniae* is grown in the presence of exogenous fatty acids, the free fatty acids are funneled to SPD_0044 via a fatty acid kinase and phosphate acyltransferase, resulting in the accumulation of the long-chain acyl-ACP. The acyl moiety makes ACP bind to FabT via more extensive hydrophobic interactions, which eventually induce significant conformational changes at the DNA-binding domains of FabT (Fig. 6B). In fact, the two DNA recognition helices shift from ~ 26 Å in the apo-form FabT to ~ 30 Å in the acyl-ACP-bound form, as calculated by 100-ns molecular dynamics simulations. The stable FabT-(acyl-ACP) complex adopts a conformation more complementary to a successive DNA major groove, and gains a higher affinity toward the target DNA, thus becomes a stronger brake to further attenuate or even shut-down the expression of downstream genes (Fig. 6C). In the presence of exogenous fatty acids, the *fab* genes are repressed by FabT together with the long-chain acyl-ACP ligand, which results in almost complete blockage of futile *de novo* FAS. This model is in agreement with a previous report that exogenous oleic acids completely block the FAS of *S. pneumoniae* [52].

In summary, the long-chain acyl-ACP is not only the intermediate of phospholipid synthesis pathway

but also a co-repressor of the global transcription repressor FabT, thus acting as a key node of the repression network that finely tunes FAS. These findings provide a distinct mechanism from the previously reported MarR family members and help us to better understand the transcriptional regulation of bacterial FAS.

Acknowledgements

This work is supported by the National Natural Science Foundation of China (Grant No. 31570728, 21573205) and Anhui Provincial Natural Science Foundation (Grant No. 1808085QC84). We appreciate the assistance of the staff at the Shanghai Synchrotron Radiation Facility (SSRF) and the Core Facility Center for Life Sciences at University of Science and Technology of China.

Data availability

Research data pertaining to this article are located at figshare.com: <https://dx.doi.org/10.6084/m9.figshare.8797580>

Author contributions

GZ, ZPC, CZZ, and QL conceived and designed the experiments; GZ, ZPC, and CD performed the experiments; GZ, YLJ, and ZZ (Zhongliang Zhu) solved the structure; GZ, ZPC, YC, ZZ (Zhiyong Zhang), CZZ, and QL analyzed the data; GZ, CZZ, and QL wrote the manuscript.

References

- Zhang YM and Rock CO (2008) Membrane lipid homeostasis in bacteria. *Nat Rev Microbiol* **6**, 222–233.

- 2 Marrakchi H, Zhang YM and Rock CO (2002) Mechanistic diversity and regulation of type II fatty acid synthesis. *Biochem Soc Trans* **30**, 1050–1055.
- 3 Graber R, Sumida C and Nunez EA (1994) Fatty acids and cell signal transduction. *J Lipid Mediat Cell Signal* **9**, 91–116.
- 4 Campbell JW and Cronan JE Jr (2001) Bacterial fatty acid biosynthesis: targets for antibacterial drug discovery. *Annu Rev Microbiol* **55**, 305–332.
- 5 Smith S, Witkowski A and Joshi AK (2003) Structural and functional organization of the animal fatty acid synthase. *Prog Lipid Res* **42**, 289–317.
- 6 White SW, Zheng J, Zhang YM and Rock CO (2005) The structural biology of type II fatty acid biosynthesis. *Annu Rev Biochem* **74**, 791–831.
- 7 Prescott DJ and Vagelos PR (1972) Acyl carrier protein. *Adv Enzymol Relat Areas Mol Biol* **36**, 269–311.
- 8 Parsons JB and Rock CO (2013) Bacterial lipids: metabolism and membrane homeostasis. *Prog Lipid Res* **52**, 249–276.
- 9 Miller DJ, Zhang YM, Subramanian C, Rock CO and White SW (2010) Structural basis for the transcriptional regulation of membrane lipid homeostasis. *Nat Struct Mol Biol* **17**, 971–975.
- 10 Heath RJ and Rock CO (1995) Regulation of malonyl-CoA metabolism by acyl-acyl carrier protein and beta-ketoacyl-acyl carrier protein synthases in *Escherichia coli*. *J Biol Chem* **270**, 15531–15538.
- 11 Schujman GE and de Mendoza D (2005) Transcriptional control of membrane lipid synthesis in bacteria. *Curr Opin Microbiol* **8**, 149–153.
- 12 Davis MS and Cronan JE Jr (2001) Inhibition of *Escherichia coli* acetyl coenzyme A carboxylase by acyl-acyl carrier protein. *J Bacteriol* **183**, 1499–1503.
- 13 Heath RJ and Rock CO (1996) Inhibition of beta-ketoacyl-acyl carrier protein synthase III (FabH) by acyl-acyl carrier protein in *Escherichia coli*. *J Biol Chem* **271**, 10996–11000.
- 14 Heath RJ and Rock CO (1996) Regulation of fatty acid elongation and initiation by acyl-acyl carrier protein in *Escherichia coli*. *J Biol Chem* **271**, 1833–1836.
- 15 Jiang P and Cronan JE (1994) Inhibition of fatty-acid synthesis in *Escherichia coli* in the absence of phospholipid-synthesis and release of inhibition by thioesterase action. *J Bacteriol* **176**, 2814–2821.
- 16 Zhu K, Zhang YM and Rock CO (2009) Transcriptional regulation of membrane lipid homeostasis in *Escherichia coli*. *J Biol Chem* **284**, 34880–34888.
- 17 Henry MF and Cronan JE Jr (1992) A new mechanism of transcriptional regulation: release of an activator triggered by small molecule binding. *Cell* **70**, 671–679.
- 18 Campbell JW and Cronan JE Jr (2001) *Escherichia coli* FadR positively regulates transcription of the *fabB* fatty acid biosynthetic gene. *J Bacteriol* **183**, 5982–5990.
- 19 Zhang YM, Marrakchi H and Rock CO (2002) The FabR (YijC) transcription factor regulates unsaturated fatty acid biosynthesis in *Escherichia coli*. *J Biol Chem* **277**, 15558–15565.
- 20 Schujman GE, Paoletti L, Grossman AD and de Mendoza D (2003) FapR, a bacterial transcription factor involved in global regulation of membrane lipid biosynthesis. *Dev Cell* **4**, 663–672.
- 21 Marrakchi H, Choi KH and Rock CO (2002) A new mechanism for anaerobic unsaturated fatty acid formation in *Streptococcus pneumoniae*. *J Biol Chem* **277**, 44809–44816.
- 22 Marrakchi H, Dewolf WE Jr, Quinn C, West J, Polizzi BJ, So CY, Holmes DJ, Reed SL, Heath RJ, Payne DJ *et al.* (2003) Characterization of *Streptococcus pneumoniae* enoyl-(acyl-carrier protein) reductase (FabK). *Biochem J* **370**, 1055–1062.
- 23 Lu YJ and Rock CO (2006) Transcriptional regulation of fatty acid biosynthesis in *Streptococcus pneumoniae*. *Mol Microbiol* **59**, 551–566.
- 24 Osterman A and Overbeek R (2003) Missing genes in metabolic pathways: a comparative genomics approach. *Curr Opin Chem Biol* **7**, 238–251.
- 25 Xu GY, Tam A, Lin L, Hixon J, Fritz CC and Powers R (2001) Solution structure of *B. subtilis* acyl carrier protein. *Structure* **9**, 277–287.
- 26 Cronan JE Jr and Subrahmanyam S (1998) FadR, transcriptional co-ordination of metabolic expediency. *Mol Microbiol* **29**, 937–943.
- 27 Jerga A and Rock CO (2009) Acyl-Acyl carrier protein regulates transcription of fatty acid biosynthetic genes via the FabT repressor in *Streptococcus pneumoniae*. *J Biol Chem* **284**, 15364–15368.
- 28 Otwinowski Z and Minor W (1997) Processing of X-ray diffraction data collected in oscillation mode. *Methods Enzymol* **276**, 307–326.
- 29 Brodersen DE, de la Fortelle E, Vornrhein C, Bricogne G, Nyborg J and Kjeldgaard M (2000) Applications of single-wavelength anomalous dispersion at high and atomic resolution. *Acta Crystallogr D Biol Crystallogr* **56**, 431–441.
- 30 Adams PD, Afonine PV, Bunkoczi G, Chen VB, Davis IW, Echols N, Headd JJ, Hung LW, Kapral GJ, Grosse-Kunstleve RW *et al.* (2010) PHENIX: a comprehensive Python-based system for macromolecular structure solution. *Acta Crystallogr D Biol Crystallogr* **66**, 213–221.
- 31 Murshudov GN, Skubak P, Lebedev AA, Pannu NS, Steiner RA, Nicholls RA, Winn MD, Long F and Vagin AA (2011) REFMAC5 for the refinement of macromolecular crystal structures. *Acta Crystallogr D Biol Crystallogr* **67**, 355–367.
- 32 Emsley P and Cowtan K (2004) Coot: model-building tools for molecular graphics. *Acta Crystallogr D Biol Crystallogr* **60**, 2126–2132.

- 33 Chen VB, Arendall WB 3rd, Headd JJ, Keedy DA, Immormino RM, Kapral GJ, Murray LW, Richardson JS and Richardson DC (2010) MolProbity: all-atom structure validation for macromolecular crystallography. *Acta Crystallogr D Biol Crystallogr* **66**, 12–21.
- 34 Flugel RS, Hwangbo Y, Lambalot RH, Cronan JE Jr and Walsh CT (2000) Holo-(acyl carrier protein) synthase and phosphopantetheinyl transfer in *Escherichia coli*. *J Biol Chem* **275**, 959–968.
- 35 Jiang YF, Chan CH and Cronan JE (2006) The soluble acyl-acyl carrier protein synthetase of *Vibrio harveyi* B392 is a member of the medium chain acyl-CoA synthetase family. *Biochemistry* **45**, 10008–10019.
- 36 van Zundert GCP, Rodrigues J, Trellet M, Schmitz C, Kastiris PL, Karaca E, Melquiond ASJ, van Dijk M, de Vries SJ and Bonvin A (2016) The HADDOCK2.2 web server: user-friendly integrative modeling of biomolecular complexes. *J Mol Biol* **428**, 720–725.
- 37 Ma XX, Guo PC, Shi WW, Luo M, Tan XF, Chen YX and Zhou CZ (2011) Structural plasticity of the thioredoxin recognition site of yeast methionine S-sulfoxide reductase Mxr1. *J Biol Chem* **286**, 13430–13437.
- 38 Otani H, Stogios PJ, Xu XH, Nocek B, Li SN, Savchenko A and Eltis LD (2016) The activity of CouR, a MarR family transcriptional regulator, is modulated through a novel molecular mechanism. *Nucleic Acids Res* **44**, 595–607.
- 39 Kumaraswami M, Schuman JT, Seo SM, Kaatz GW and Brennan RG (2009) Structural and biochemical characterization of MepR, a multidrug binding transcription regulator of the *Staphylococcus aureus* multidrug efflux pump MepA. *Nucleic Acids Res* **37**, 1211–1224.
- 40 Andresen C, Jalal S, Aili D, Wang Y, Islam S, Jarl A, Liedberg B, Wretling B, Martensson LG and Sunnerhagen M (2010) Critical biophysical properties in the *Pseudomonas aeruginosa* efflux gene regulator MexR are targeted by mutations conferring multidrug resistance. *Protein Sci* **19**, 680–692.
- 41 Dolan KT, Duguid EM and He C (2011) Crystal structures of SlyA protein, a master virulence regulator of *Salmonella*, in free and DNA-bound states. *J Biol Chem* **286**, 22178–22185.
- 42 Zheng G, Lu XJ and Olson WK (2009) Web 3DNA—a web server for the analysis, reconstruction, and visualization of three-dimensional nucleic-acid structures. *Nucleic Acids Res* **37**, W240–W246.
- 43 Deochand DK and Grove A (2017) MarR family transcription factors: dynamic variations on a common scaffold. *Crit Rev Biochem Mol Biol* **52**, 595–613.
- 44 Holm L and Laakso LM (2016) Dali server update. *Nucleic Acids Res* **44**, W351–W355.
- 45 Poole K, Tetro K, Zhao Q, Neshat S, Heinrichs DE and Bianco N (1996) Expression of the multidrug resistance operon *mexA-mexB-oprM* in *Pseudomonas aeruginosa*: *mexR* encodes a regulator of operon expression. *Antimicrob Agents Chemother* **40**, 2021–2028.
- 46 Anandapadamanaban M, Pilstal R, Andresen C, Trehwella J, Moche M, Wallner B and Sunnerhagen M (2016) Mutation-induced population shift in the MexR conformational ensemble disengages DNA binding: a novel mechanism for MarR family derepression. *Structure* **24**, 1311–1321.
- 47 Birukou I, Seo SM, Schindler BD, Kaatz GW and Brennan RG (2014) Structural mechanism of transcription regulation of the *Staphylococcus aureus* multidrug efflux operon *mepRA* by the MarR family repressor MepR. *Nucleic Acids Res* **42**, 2774–2788.
- 48 Chovancova E, Pavelka A, Benes P, Strnad O, Brezovsky J, Kozlikova B, Gora A, Sustar V, Klvana M, Medek P *et al.* (2012) CAVER 3.0: a tool for the analysis of transport pathways in dynamic protein structures. *PLoS Comput Biol* **8**, e1002708.
- 49 Alekshun MN and Levy SB (1997) Regulation of chromosomally mediated multiple antibiotic resistance: the *mar* regulon. *Antimicrob Agents Chemother* **41**, 2067–2075.
- 50 Grove A (2013) MarR family transcription factors. *Curr Biol* **23**, R142–R143.
- 51 Zhu L, Zou Q, Cao X and Cronan JE (2019) *Enterococcus faecalis* encodes an atypical auxiliary acyl carrier protein required for efficient regulation of fatty acid synthesis by exogenous fatty acids. *MBio* **10**, e00577–19.
- 52 Parsons JB, Frank MW, Subramanian C, Saenkham P and Rock CO (2011) Metabolic basis for the differential susceptibility of Gram-positive pathogens to fatty acid synthesis inhibitors. *Proc Natl Acad Sci USA* **108**, 15378–15383.